CONFIDENTIAL

Copy 417
RM L55B10

NACA RM L55B10

NACA



# RESEARCH MEMORANDUM

## LIFT, DRAG, AND LONGITUDINAL STABILITY AT MACH NUMBERS FROM 0.8 TO 2.1 OF A ROCKET-POWERED MODEL HAVING A TAPERED UNSWEPT WING OF ASPECT RATIO 3 AND INLINE TAIL SURFACES

By Warren Gillespie, Jr.

Langley Aeronautical Laboratory
Langley Field, Va.



CLASSIFIED DOCUMENT



NATIONAL ADVISORY COMMITTEE FOR AERONAUTICS

WASHINGTON

April 25, 1955

CONFIDENTIAL

NATIONAL ADVISORY COMMITTEE FOR AERONAUTICS

RESEARCH MEMORANDUM

# LIFT, DRAG, AND LONGITUDINAL STABILITY AT MACH NUMBERS FROM 0.8 TO 2.1 OF A ROCKET-POWERED MODEL HAVING A TAPERED UNSWEPT WING OF ASPECT RATIO 3 AND INLINE TAIL SURFACES

By Warren Gillespie, Jr.

## SUMMARY

An investigation was made of a configuration having a body of fineness ratio 16.9, an unswept wing of aspect ratio 3 and a taper ratio 0.4, and inline tail surfaces which was aeropulsed continuously in pitch during free flight with and without a sustainer rocket motor operating. The Mach number range covered by the investigation was from 0.8 to 2.1. Zero-lift drag and drag-due-to-lift data were obtained during coasting flight of the model. Normal force, pitching moment, static longitudinal stability, and downwash and wake effects at the horizontal tail were obtained with and without the rocket motor thrusting.

Drag due to lift at a Mach number of 2.0 was approximately two times the minimum value of 0.155 near a Mach number of 0.97. The variation of lift with angle of attack was linear at supersonic Mach numbers. The variation of pitching moment with lift, however, was nonlinear up to a Mach number of approximately 1.3. Downwash was present at the horizontal tail up to a Mach number of about 1.5 and angles of attack greater than $2^{\circ}$. Upwash occurred at higher Mach numbers and at angles of attack between $\pm 2^{\circ}$. The maximum pressure loss at the horizontal tail due to the wing wake was 20 percent of the free-stream dynamic pressure. The continuous pitching of the model induced lateral oscillations having maximum amplitude of about $\pm 3^{\circ}$ of sideslip at low supersonic speeds.

## INTRODUCTION

In reference 1 it has been shown that the drag due to lift of unswept wings of aspect ratio 4 is reduced at a Mach number above 0.88 by decreasing the wing-section thickness. As explained in reference 1, above a Mach number of 0.88 the resultant force is normal to the wing chord, and since the thin wing has the higher lift-curve slope, it has the lower drag due

to lift. Reference 2 has presented the subsonic and supersonic lift, drag, and pitching-moment results for a tailless configuration having a 3-percent-thick unswept wing of aspect ratio 3.1, and reference 3 has determined the transonic lift and drag characteristics of the Douglas X-3 research airplane which has an unswept wing of aspect ratio 3.09 and a 4.5-percent-thick modified hexagonal section. The configuration of the present investigation was selected to extend the supersonic range of experimental lift, drag, and stability data available on airplanelike configurations employing thin unswept wings of low aspect ratio.

A rocket-propelled model having a 3-percent-thick unswept wing of aspect ratio 3 and a taper ratio of 0.4 and inline tail surfaces was flight tested at the Langley Pilotless Aircraft Research Station at Wallops Island, Va. The horizontal tail was aerodynamically pulsed between stop settings of 1.82° and -1.93°. The basic aerodynamic parameters in pitch were determined from the response of the model to the tail motion.

## SYMBOLS

$C_N$ normal-force coefficient, $\frac{a_n}{g}\frac{W/S}{q}$

$C_C$ chord-force coefficient, $\frac{-a_l}{g}\frac{W/S}{q}$

$C_L$ lift coefficient, $C_N \cos \alpha - C_C \sin \alpha$

$C_D$ drag coefficient, $C_C \cos \alpha + C_N \sin \alpha$

$C_m$ pitching-moment coefficient about center of gravity, $\frac{I_Y \ddot{\theta}}{57.3 q S \bar{c}}$

$a_n$ normal acceleration, ft/sec$^2$

$a_l$ longitudinal acceleration, ft/sec$^2$

$a_t$ transverse acceleration, ft/sec$^2$

$g$ acceleration due to gravity, 32.2 ft/sec$^2$

$q$ dynamic pressure, lb/sq ft

$V$ velocity, ft/sec

| | |
|---|---|
| $M$ | Mach number |
| $R$ | Reynolds number, where reference length is 1 ft |
| $W$ | weight of model, lb |
| $S$ | total wing area to body center line, 4.00 sq ft |
| $\bar{c}$ | wing mean aerodynamic chord, 1.22 ft |
| $\alpha$ | angle of attack, deg |
| $\theta$ | angle of pitch, deg |
| $\beta$ | angle of sideslip, deg |
| $\psi$ | angle of yaw, deg |
| $\delta$ | horizontal-tail deflection, deg |
| $\Delta P$ | differential pressure, lb/sq ft |
| $C_p$ | differential pressure coefficient, $\frac{\Delta P}{q}$ |
| $I_Y$ | moment of inertia in pitch about center of gravity, slug-ft$^2$ |
| $H$ | total pressure, lb/sq ft |
| $\epsilon$ | downwash angle at horizontal tail, deg |
| $\eta$ | ratio of dynamic pressure at horizontal tail to free-stream dynamic pressure |

One and two dots over symbols denote first and second time derivatives, respectively.

## MODEL

A two-view drawing of the test configuration is shown in figure 1. The fuselage was a body of revolution of fineness ratio 16.9. Ordinates defining the nose shape are given in table I. The geometric and mass characteristics of the model are listed in table II. The maximum body-diameter—wing-span ratio was 0.169. An unswept wing (75-percent-chord line straight) of aspect ratio 3 and taper ratio 0.4 and having a 3-percent-thick hexagonal airfoil section was mounted on the body center line in

line with the horizontal tail which was mass balanced and pivoted about the 0.55-exposed-mean-aerodynamic-chord point.

The model was of metal construction with a solid 7075-T6 (formerly 75S-T6) aluminum-alloy wing. A sustainer rocket motor was carried inside the fuselage in addition to a telemeter with angle-of-attack, angle-of sideslip, pressure, and accelerometer instruments. The model and its booster are pictured in the launching attitude in figure 2.

## TESTS

Prior to the flight test the wing of the model was static tested to determine the streamwise wing twist due to loading concentrated along the 40-percent-chord line. The twist was found to be negligible. Therefore the experimental results of the test should be very closely equal to "rigid wing" values.

Data were obtained during ascent of the model after separation from the booster. During flight of the model alone, a square-wave pulse was continuously generated as the tail automatically flipped between stop settings due to a reversal in direction of the tail lift. The technique is described more fully in reference 4.

The quantities measured by the telemeter system were normal and longitudinal accelerations, angles of attack and sideslip, horizontal-tail deflection, free-stream total pressure and a differential pressure on the horizontal tail. The velocity obtained from CW Doppler radar was used in conjunction with tracking radar and radiosonde data to calculate Mach number, Reynolds number, and dynamic pressure experienced by the model during flight. The variation of the free-stream Reynolds number per foot length and dynamic pressure with Mach number is shown in figure 3(a). The model experienced a coasting period before and after the period of flight with the sustainer motor thrusting. The ranges of the maximum angles of attack and induced sideslip during the test are shown in figure 3(b).

## ACCURACY

The random error in the data is indicated by the scatter of the experimental points which is generally much less at the highest dynamic pressures or Mach numbers. The probable random error of a telemetered quantity obtained from a single instrument is approximately 1 percent.

Presented below are the ranges of the telemeter instruments used in the test model:

| | |
|---|---|
| Nose angle-of-attack indicator, deg | ±10 |
| Nose angle-of-sidelsip indicator, deg | ±3 |
| Vertical-tail angle-of-sideslip indicator, deg | ±4 |
| Normal accelerometer at the nose, g units | ±30 |
| Normal accelerometer near the center of gravity, g units | ±40 |
| Longitudinal accelerometer, g units | +1 to -8 |
| Total-pressure indicator at nose, lb/sq in. | 14 to 90 |
| Total-pressure indicator at horizontal tail, lb/sq in. | 14 to 90 |
| Differential-pressure indicator at horizontal tail, lb/sq in. | ±20 |
| Horizontal-tail-position indicator, deg | ±2.2 |

Because of the low range of the longitudinal accelerometer, this instrument can be affected by interaction with normal acceleration. The interaction may arise both from angular misalinement of the instrument mounting base and also from construction inaccuracies inside the instrument. Examination of plots of the longitudinal-acceleration data against normal-acceleration data from the flight of the test model indicated a probable effective angular misalinement of about 1° for the longitudinal accelerometer. The effect of this interaction on the determination of drag due to lift is discussed later in the section on drag.

An additional source of inaccuracy in the final results may be cross-coupling effects of induced yawing and rolling motion. These effects as indicated by figure 3(b) would be expected to be greatest at the low supersonic speeds of the test.

## CORRECTIONS

Measurements obtained from the wind-vane instruments were corrected for position error resulting from flight-path curvature as follows:

$$\alpha = \alpha_{measured} + \frac{6.50}{V}\dot{\theta}$$

$$\beta = \beta_{measured\ at\ nose} - \frac{6.50}{V}\dot{\psi}$$

$$\beta = \beta_{measured\ at\ tail} + \frac{2.17}{V}\dot{\psi}$$

Position corrections were also made to measurements obtained from the normal and longitudinal accelerometers mounted near the center of gravity of the model as follows:

$$\frac{a_n}{g} = \left(\frac{a_n}{g}\right)_{measured} + \frac{0.258}{32.2(57.3)^2}\dot{\theta}^2$$

$$\frac{a_l}{g} = \left(\frac{a_l}{g}\right)_{measured} + \frac{0.175}{32.2}\left(\ddot{\theta} + \ddot{\beta}\right)$$

## RESULTS AND DISCUSSION

### Drag

Figure 4 shows a typical variation of drag coefficient with lift coefficient squared and also with lift coefficient at a Mach number of 1.85. The data points of the upper plot of drag coefficient against lift coefficient squared do not fall on a single line as they should do for a basically symmetrical configuration, and the corresponding drag polar is not symmetrical about zero lift coefficient. These irregularities, as mentioned previously, are believed to be mostly due to normal-force interaction with the longitudinal accelerometer. Examination of plots of $C_C$ against $C_N$ over the Mach number range of the tests indicated a probable effective angular misalinement of about 1° for the longitudinal accelerometer. The flagged symbols of figure 4 have been corrected for this interaction. The corrected values agree well with the dashed line which was determined from the average of the uncorrected points in the upper plot of figure 4. Rather than correct each data point for this interaction effect, plots of drag coefficient against lift coefficient squared were made over the Mach number range and an average line was determined for each plot from the upper and lower sets of points. Drag due to lift was determined from the slope of the average line and the minimum drag was taken to occur at zero lift where the line intersects the axis.

The minimum drag at zero lift and the drag due to lift over the angle-of-attack range shown in figure 3(b) are presented separately in figure 5. The wing-with-interference drag at zero lift was determined as the difference between the drag of the test model and that of the wingless model of reference 5. A further comparison with the body model of reference 6 at Mach number 1.74 shows the drag contributions due to the body and the body base. The plot of drag due to lift shows that near a Mach number of 0.97 a minimum value of 0.155 occurred. A value approximately two times the minimum value occurred at a Mach number of 2.0.

The drag due to lift was very closely approximated by the expression $1/57.3C_{N_\alpha}$. It is interesting to note that the drag due to lift for the body-tail model of reference 5 shows the same trend and is only slightly higher than that for the winged configuration when the latter is based on the sum of the wing and horizontal-tail areas. The wing-body model of reference 2 is also shown for comparison. For this model the drag due to lift is lower at low supersonic Mach numbers and higher at high supersonic Mach numbers than the drag due to lift of the test model based on the sum of the wing and horizontal-tail areas. This difference may be partly due to the change in flow conditions at the horizontal tail of the test model. A condition of downwash at the tail would be expected to increase the drag due to lift.

## Normal Force and Pitching Moment

Figures 6 to 8 present plots of normal-force and pitching-moment coefficients and summarize the variation of the normal-force- and pitching-moment-curve slopes with Mach number. Except for the lowest average Mach number of 0.98, figure 6 shows that the variation of normal-force coefficient with angle of attack is linear within the range tested. The variation of pitching-moment coefficient with normal-force coefficient is markedly nonlinear at the low test Mach numbers up to a Mach number of about 1.3 but, as shown in figure 7, this variation becomes linear at the higher test Mach numbers. The variation of the normal-force-coefficient slope $C_{N_\alpha}$ with Mach number presented in figure 8 is similar to the variation for the wingless model of reference 5. The contribution of the wing with interference was determined as the difference between the curves of the two models. The variation of the static-stability parameter $dC_m/dC_N$ with Mach number is also shown in figure 8. The model at zero lift was unstable below about Mach number 1.08 with the static stability increasing with both Mach number and lift. The wingless model of reference 5 showed negligible change of stability with lift and a forward movement of the aerodynamic center with increasing supersonic Mach numbers. A comparison is made with the stability results from the wind-tunnel model of reference 2. This tailless model had a similar wing plan form with a 3-percent-thick section. Addition of the inline tail to the present model appears to have increased the nonlinear region of static stability over that obtained from the tailless configuration.

## Flow Conditions at the Horizontal Tail

Figure 9 shows that up to a Mach number of about 1.5 and angles of attack greater than $2^\circ$ and less than $-2^\circ$ the horizontal tail operated in

a region of downwash. At higher Mach numbers and angles of attack between $\pm 2^\circ$ an average upwash was present. The change from downwash to upwash at the beginning of tail flip may be due to a decrease of the wing downwash (which interacts with the body upwash) as the supersonic Mach number increased. Figure 10 presents the variation of local downwash determined from the differential pressure measured at the exposed mean aerodynamic chord of the tail with angle of attack. Local downwash was calculated from the expression $\epsilon = \alpha + \delta - KC_p$. The factor K was determined from the change in the differential pressure when the tail flipped. The variation of the local downwash evaluated in this manner is nonlinear. The local downwash agrees well with the points of average downwash obtained from the angle of attack at which the tail flipped.

Figure 11 shows the pressure loss at the exposed mean aerodynamic chord of the horizontal tail that occurred when the tail passed through the wake from the wing. There was a maximum loss of about 20 percent of free-stream dynamic pressure. The extent of the pressure loss with angle of attack follows the downwash trend of figure 9.

## Buffeting and Model Vibrations

The normal-accelerometer traces of figure 12 which are portions of the telemeter record during the first and second coasting periods show that buffeting developed near a Mach number of 0.9 when the angle of attack exceeded $-10.4^\circ$ and the normal-force coefficient reached values of -1.16 and -1.50, respectively. Buffeting did not occur at higher Mach numbers. In particular, buffeting did not occur at a Mach number of 0.95 during the first coasting period when the angle of attack reached $10.3^\circ$ nor at a Mach number of 0.94 during the second coasting period when the angle of attack exceeded $11.6^\circ$. The X-3 rocket model of reference 7 which had a 4.5-percent-thick wing of similar section and plan form developed a similar case of buffeting below a Mach number of 0.9 when the angle of attack exceeded $9^\circ$ or $10^\circ$.

The test model was plagued by a disturbance each time the angle of attack and normal acceleration changed sign. This is clearly evident in figure 12(a). This disturbance caused the two low-range transverse accelerometers to vibrate at a structural natural frequency of the body. Vibration of the flow indicator mounted on the lower vertical tail also occurred. The frequency of this vibration was approximately constant and is probably some structural frequency of the vertical-tail fin. At 6.7 seconds flight time the frequency of the transverse-accelerometer vibrations at the model center of gravity momentarily changed to the same frequency as that of the flow indicator.

## Cross Coupling

A resonant buildup of sideslip angle occurred each of the three times that the model traversed the low supersonic Mach number region. The amplitude of the lateral motion was not primarily a function of the angle of attack. As shown by figure 3(b) the sideslip amplitude was quite small at the lowest test Mach numbers where the amplitude of angle of attack was relatively very large. Figure 13 shows a typical buildup of the induced sideslip motion. The periods of oscillation in pitch and sideslip are approximately the same with the sideslip lagging by one-eighth of an oscillation. The angle $\Delta\beta$ was calculated by subtracting the sideslip obtained from the flow indicator at the lower vertical tail from the sideslip obtained from the indicator at the nose. Due to the offset position of the rear flow indicator, values of $\Delta\beta$ when the angle of attack was either zero or positive or when the angle of sideslip was zero should indicate sidewash due to the model rolling. When the angle of attack was negative and the sideslip angle not zero, sidewash due to sideslip at angles of attack may also be indicated. The sudden variation of $\Delta\beta$ at negative angles of attack shown in figure 13 is attributed to sidewash due to sideslip. The short-dash line was drawn to indicate the probable variation of $\Delta\beta$ in the absence of such sidewash. The resulting variation of $\Delta\beta$ indicates a rolling oscillation of the model.

The variations that occurred in the angle-of-attack response of the wingless model of reference 5 did not occur for the winged model of the present test. The reason for the difference appears to be that the reference model probably experienced a more or less steady roll rate during cross coupling, whereas the present test model oscillated in roll.

## CONCLUSIONS

An investigation of lift, drag, and stability of a rocket-propelled model having an unswept wing of aspect ratio 3 and taper ratio 0.4 and inline tail surfaces leads to the following conclusions:

1. Drag due to lift at a Mach number of 2.0 was approximately two times the minimum value of 0.155 near a Mach number of 0.97. The expression $1/57.3C_{N_\alpha}$ (where $C_{N_\alpha}$ is the slope of the normal-force-coefficient curve) closely approximated the drag due to lift.

2. The variation of lift with angle of attack was linear at supersonic Mach numbers over the range of lift covered by the test.

3. The variation of pitching moment with lift was nonlinear up to a Mach number of approximately 1.3.

4. Downwash was present at the horizontal tail up to a Mach number of about 1.5 and angles of attack greater than $2^{\circ}$ and less than $-2^{\circ}$. Upwash occurred at higher Mach numbers and angles of attack less than $2^{\circ}$ and greater than $-2^{\circ}$. The maximum loss in free-stream dynamic pressure at the tail due to the wing wake was 20 percent.

5. Continuous pitching of the model induced lateral oscillations having maximum amplitude of about $\pm 3^{\circ}$ of sideslip at low supersonic speeds.

Langley Aeronautical Laboratory,
National Advisory Committee for Aeronautics,
Langley Field, Va., January 31, 1955.

## REFERENCES

1. Polhamus, Edward C.: Drag Due to Lift at Mach Numbers up to 2.0. NACA RM L53I22b, 1953.

2. Heitmeyer, John C.: Lift, Drag, and Pitching Moment of Low-Aspect-Ratio Wings at Subsonic and Supersonic Speeds - Plane Tapered Wing of Aspect Ratio 3.1 With 3-Percent-Thick Rounded-Nose Section. NACA RM A52D23, 1952.

3. Bellman, Donald R., and Murphy, Edward D.: Lift and Drag Characteristics of the Douglas X-3 Research Ariplane Obtained During Demonstration Flights to a Mach Number of 1.20. NACA RM H54I17, 1954.

4. Gillespie, Warren, Jr., and Dietz, Albert E.: Use of an Aerodynamically Pulsed All-Movable Horizontal Tail To Obtain Longitudinal Characteristics of Rocket-Powered Models in Free Flight and Some Initial Results From an Arrow-Wing-Body-Tail Configuration. NACA RM L52C10, 1952.

5. Gillespie, Warren, Jr., and Dietz, Albert E.: Rocket-Powered Model Investigation of Lift, Drag, and Stability of a Body-Tail Configuration at Mach Numbers From 0.8 to 2.3 and Angles of Attack Between $\pm 6.5^{\circ}$. NACA RM L54C04, 1954.

6. Gillespie, Warren, Jr.: Free-Flight Determination of Force and Stability Characteristics of an Inclined Body of Fineness Ratio 16.9 at a Mach Number of 1.74. NACA RM L54G28a, 1954.

7. Peck, Robert F., and Mitchell, Jesse L.: An Investigation of the Longitudinal Characteristics of the X-3 Configuration With Wing and Horizontal Tail Surfaces of Aspect Ratio 3.0 by Means of Rocket-Propelled Models. Results at High Lift Coefficients. NACA RM L51G10, 1951.

TABLE I

CONTOUR ORDINATES OF NOSE

| Station, in. from nose | Body radius, in. |
|---|---|
| 0 | 0.17 |
| .06 | .18 |
| .12 | .21 |
| .24 | .22 |
| .48 | .28 |
| .73 | .35 |
| 1.22 | .46 |
| 2.00 | .64 |
| 2.45 | .73 |
| 4.80 | 1.24 |
| 7.35 | 1.72 |
| 8.00 | 1.85 |
| 9.80 | 2.15 |
| 12.25 | 2.50 |
| 13.12 | 2.61 |
| 14.37 | 2.75 |
| 14.70 | 2.78 |
| 17.15 | 3.01 |
| 19.60 | 3.22 |
| 22.05 | 3.38 |
| 24.50 | 3.50 |
| 25.00 | 3.50 |

TABLE II

CHARACTERISTICS OF MODEL

| | |
|---|---|
| **Wing:** | |
| Span, ft | 3.46 |
| Area, sq ft | 4.0 |
| Aspect ratio | 3.0 |
| Taper ratio | 0.4 |
| Sweepback of 0.5 chord, deg | 8.2 |
| Mean aerodynamic chord, ft | 1.22 |
| Airfoil section | 3-percent-thick hexagonal |
| **Body:** | |
| Maximum diameter, ft | 0.58 |
| Base diameter, ft | 0.42 |
| Length, ft | 9.85 |
| Fineness ratio | 16.9 |
| Boattail angle, deg | 2.16 |
| **Horizontal tail:** | |
| Span, ft | 1.85 |
| Aspect ratio | 2.7 |
| Sweepback of 0.5-chord line, deg | 0 |
| Airfoil section | 4-percent-thick hexagonal |
| **Vertical tail:** | |
| Span, ft | 1.67 |
| Aspect ratio | 1.08 |
| Sweepback of L.E., deg | 70 |
| Sweepback of T.E., deg | 15 |
| Airfoil section | 1/4-inch beveled flat plate |
| **Model weight, lb** | |
| With sustainer rocket loaded | 156.0 |
| With sustainer rocket empty | 112.2 |
| **Moment of inertia in pitch, slug-ft$^2$** | |
| With sustainer rocket loaded | 25.9 |
| With sustainer rocket empty | 23.1 |
| **Center of gravity with sustainer rocket loaded or empty, percent $\bar{c}$ aft of L.E. of mean aerodynamic chord** | 38.6 |

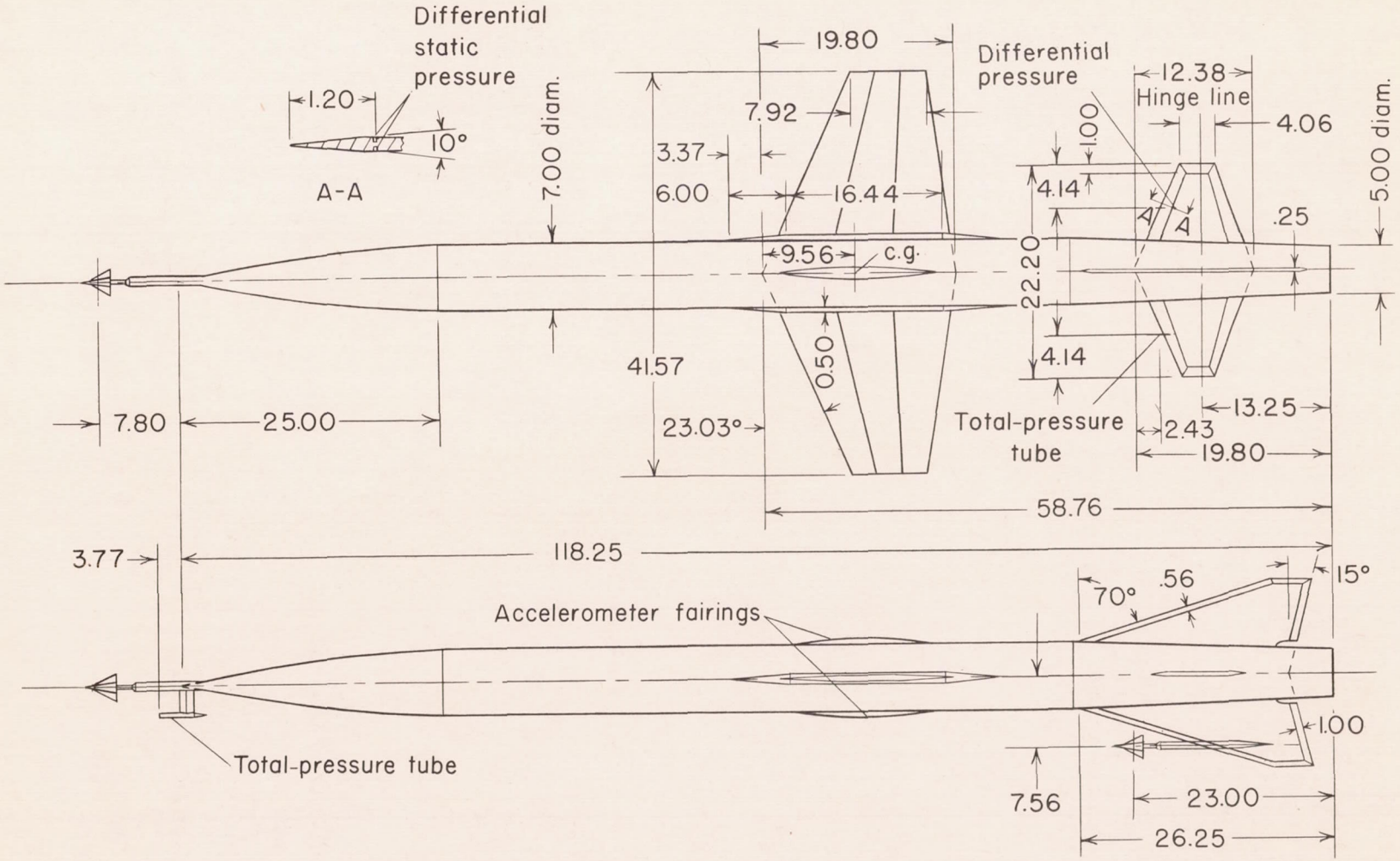


Figure 1.- Test configuration. All linear dimensions are in inches.

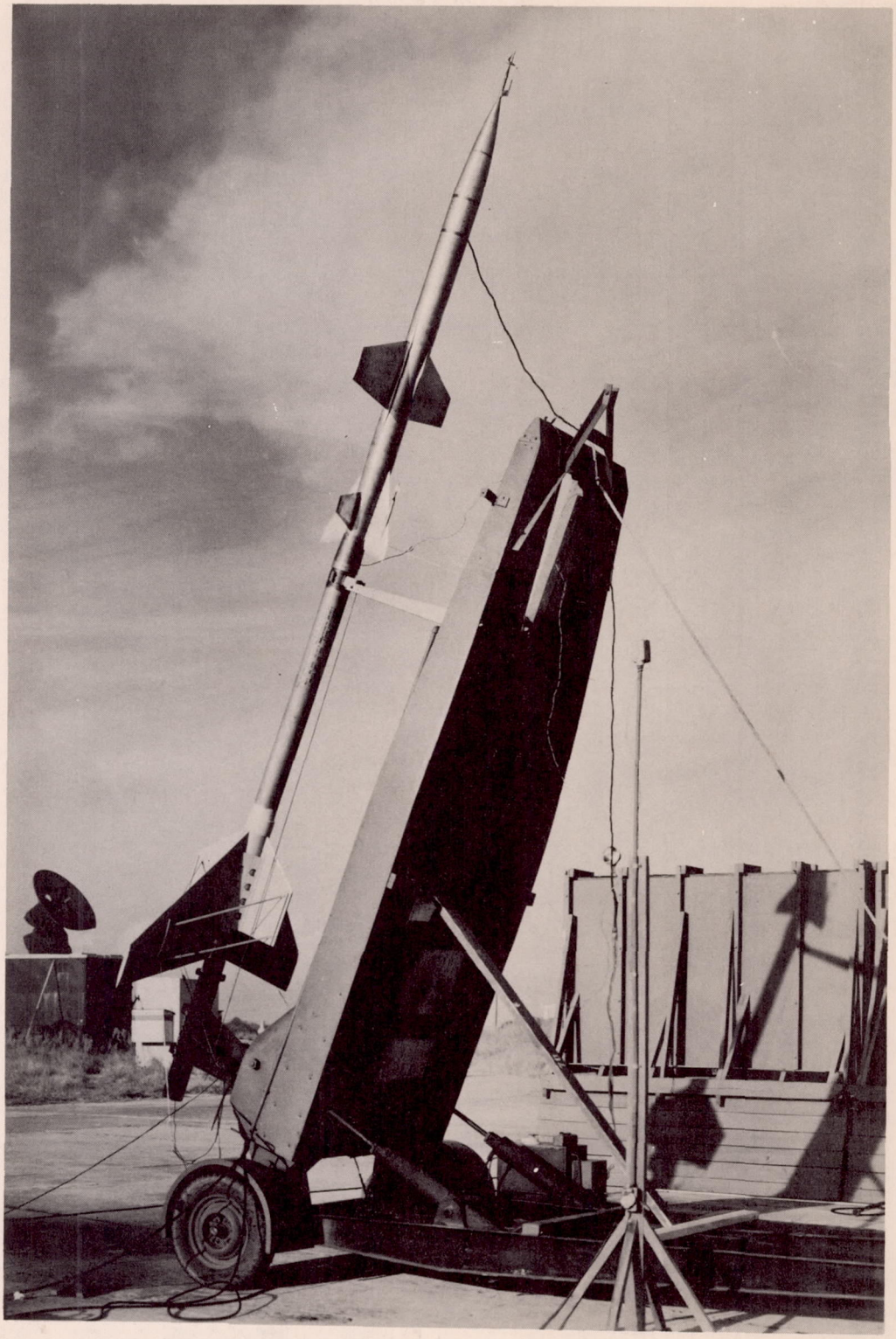

Figure 2.- Model and booster on launcher. L-82600

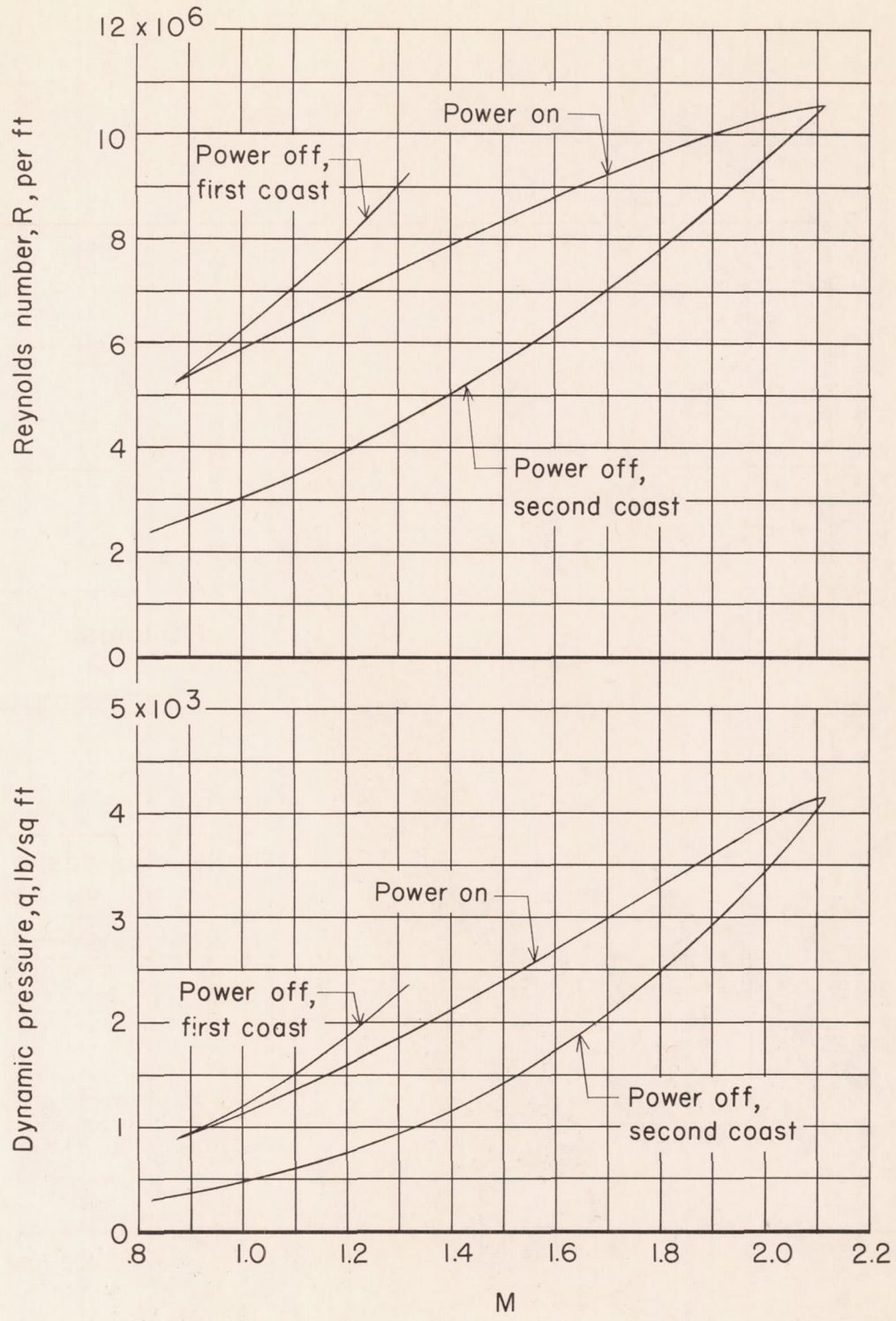


(a) Reynolds number and dynamic pressure.

Figure 3.- Flight test conditions.

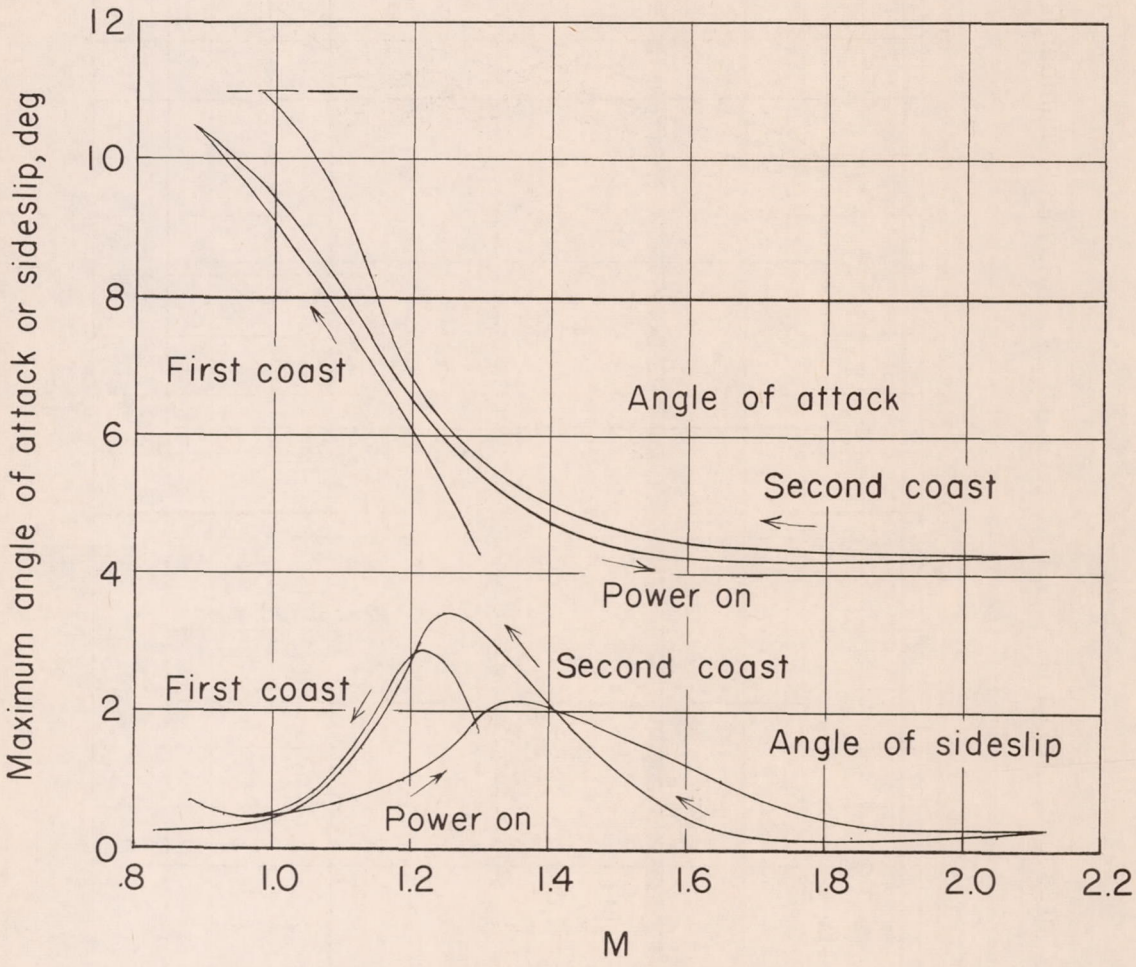


(b) Maximum angle of attack and induced sideslip.

Figure 3.- Concluded.

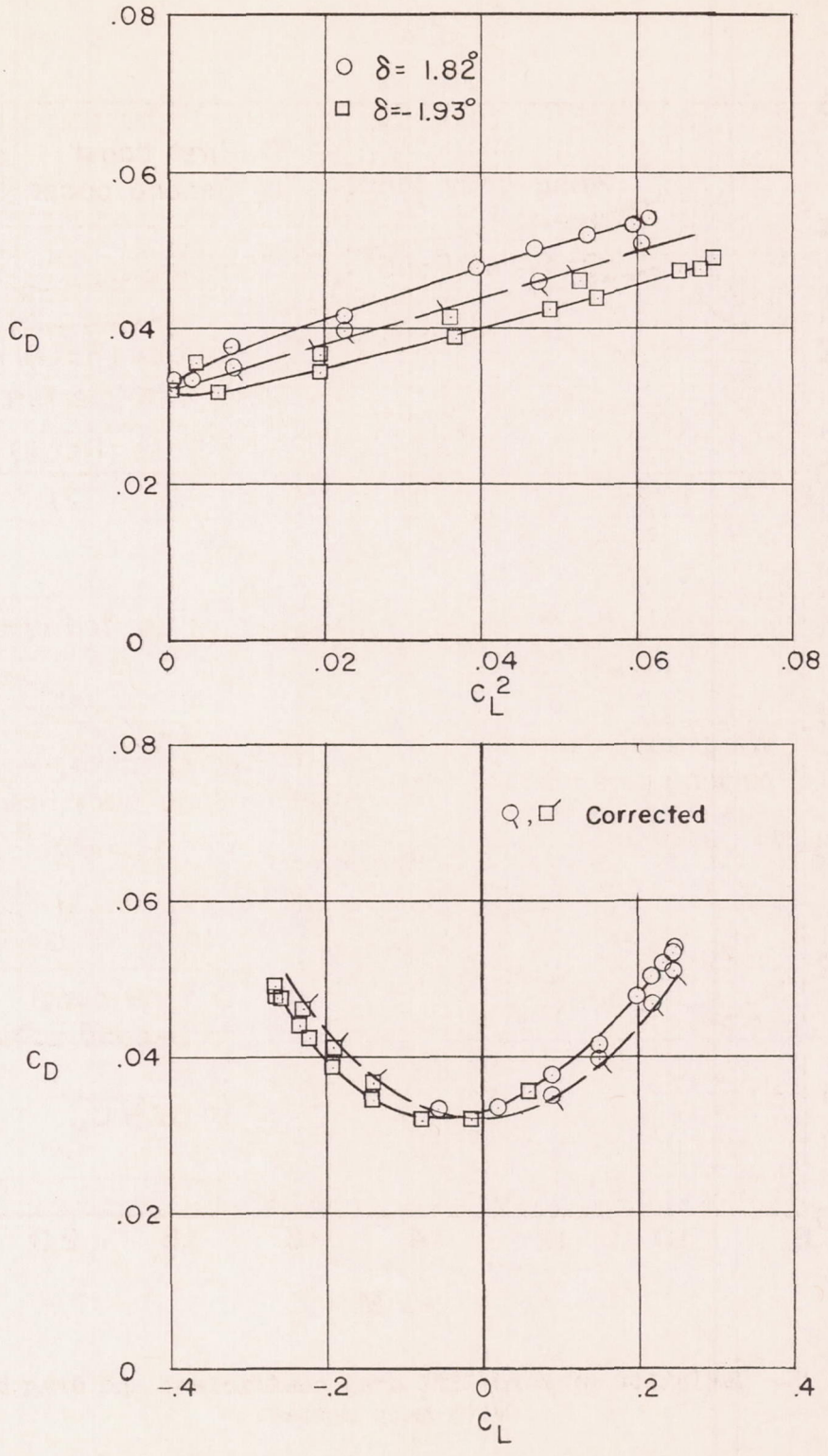


Figure 4.- Typical variation of drag coefficient with lift coefficient squared and with lift coefficient. Mach number, 1.85.

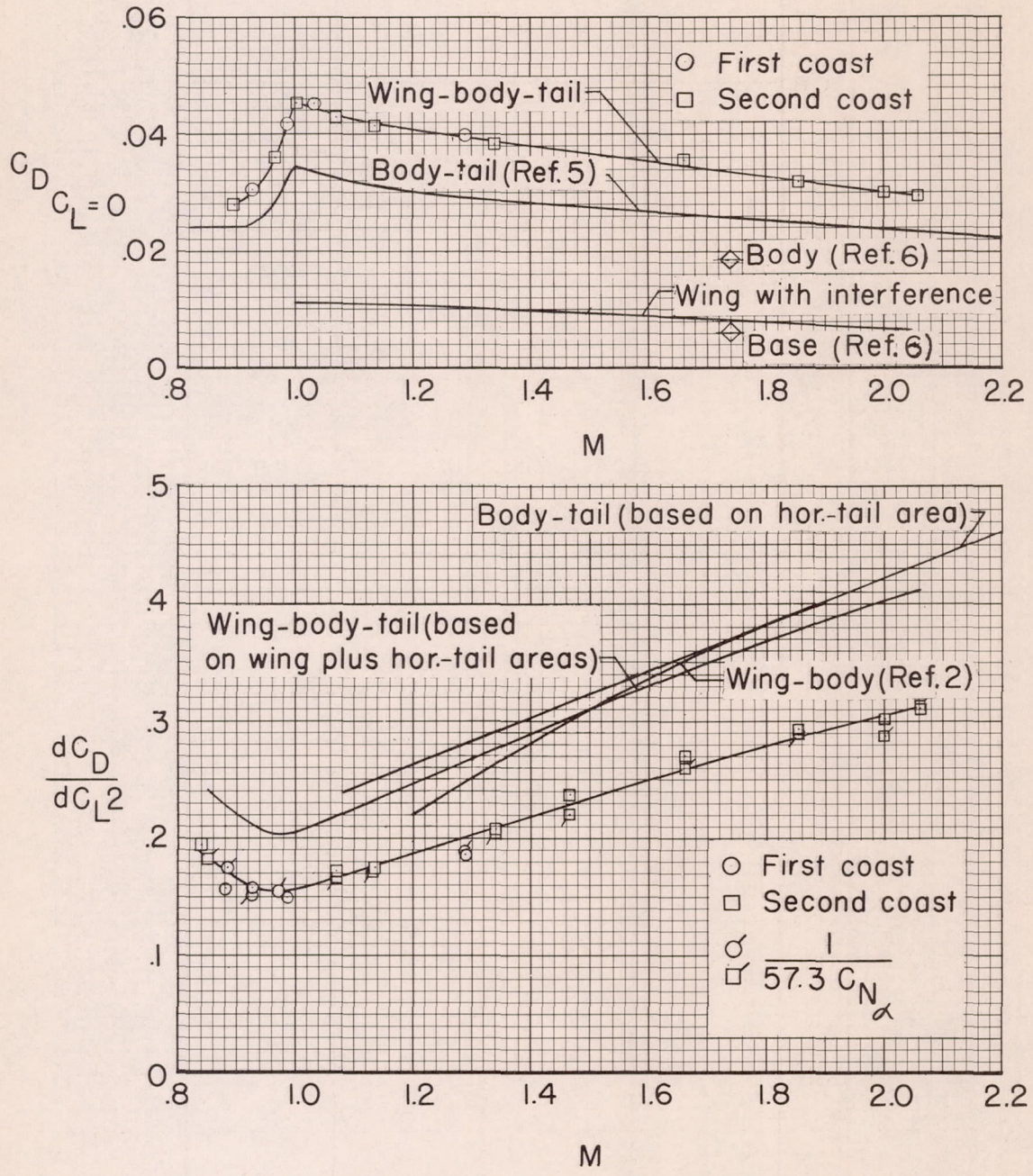


Figure 5.- Variation of zero-lift drag coefficient and drag due to lift with Mach number.

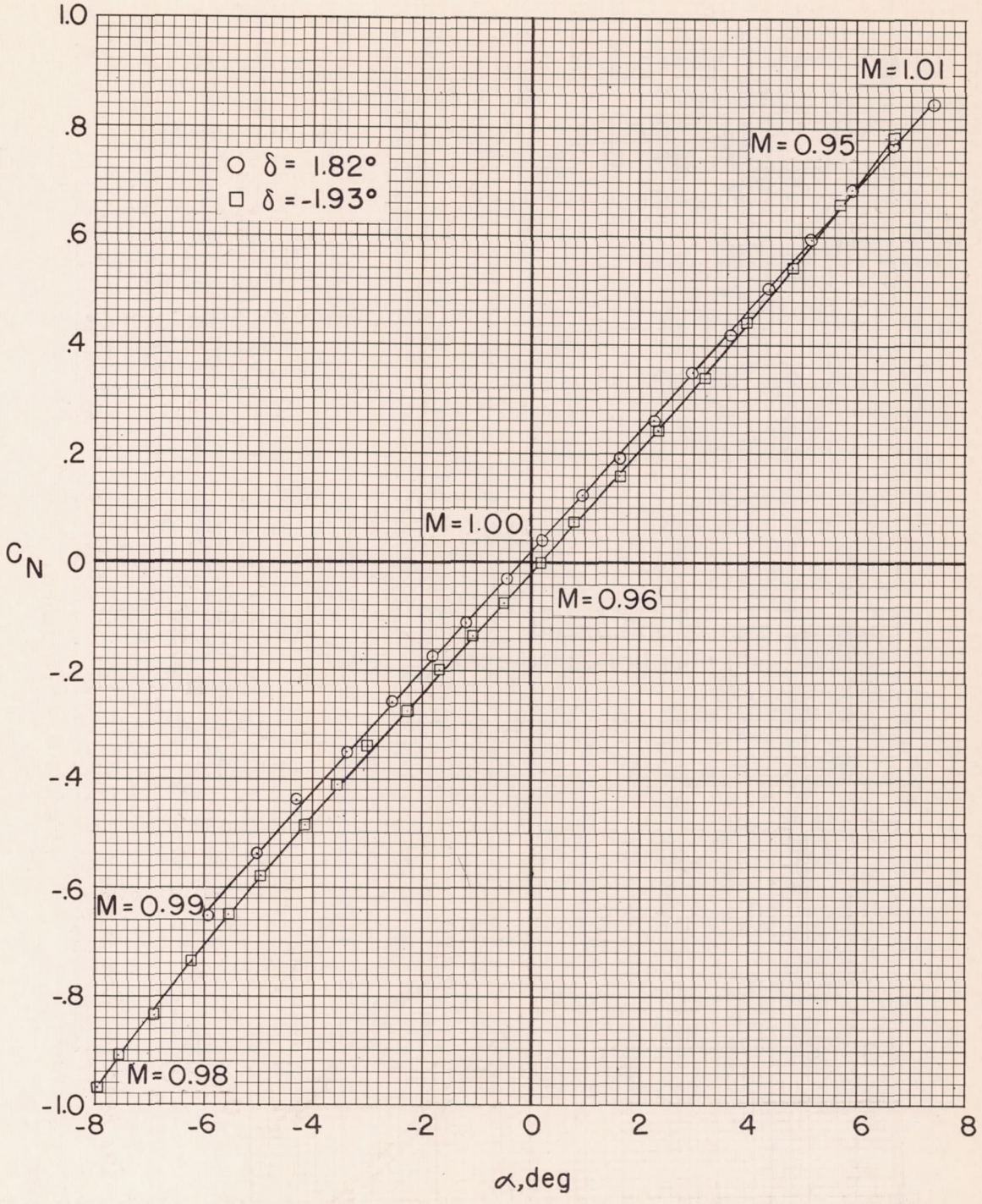


(a) Average Mach number of 0.98.

Figure 6.- Variation of normal-force coefficient with angle of attack.

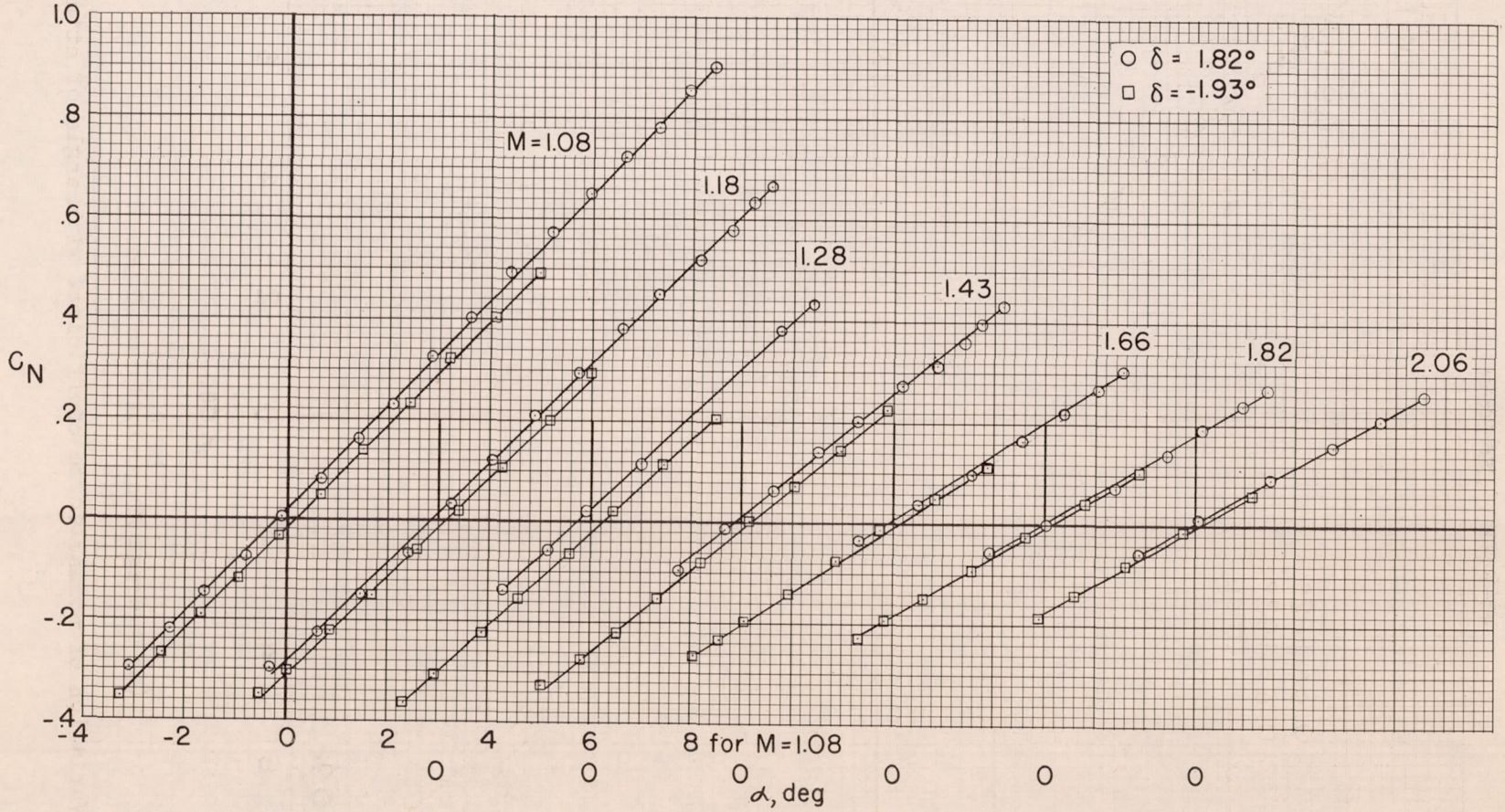


(b) Average Mach numbers of 1.08, 1.18, 1.28, 1.43, 1.66, 1.82, and 2.06.

Figure 6.- Concluded.

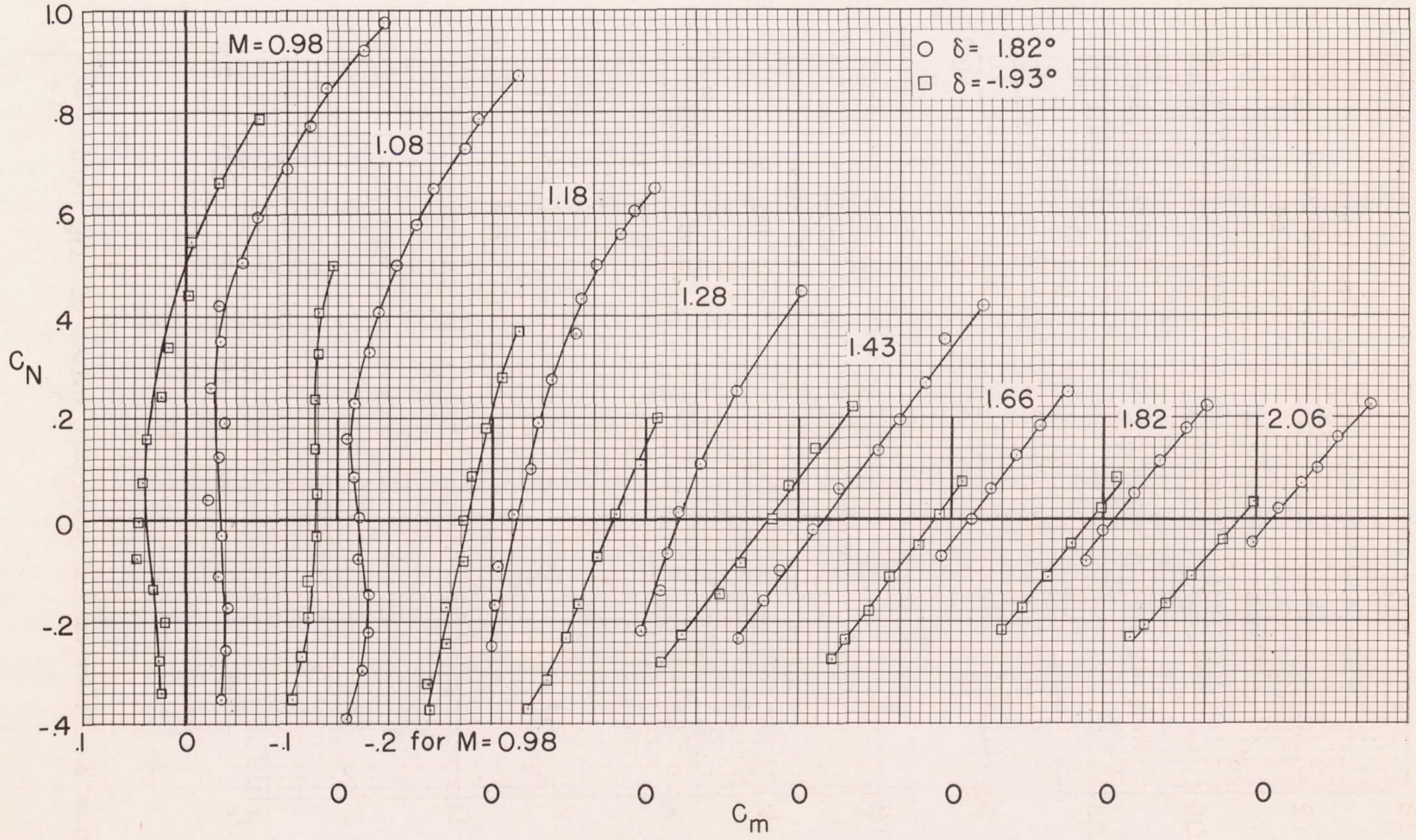


Figure 7.- Variation of pitching-moment coefficient with normal-force coefficient at various Mach numbers.

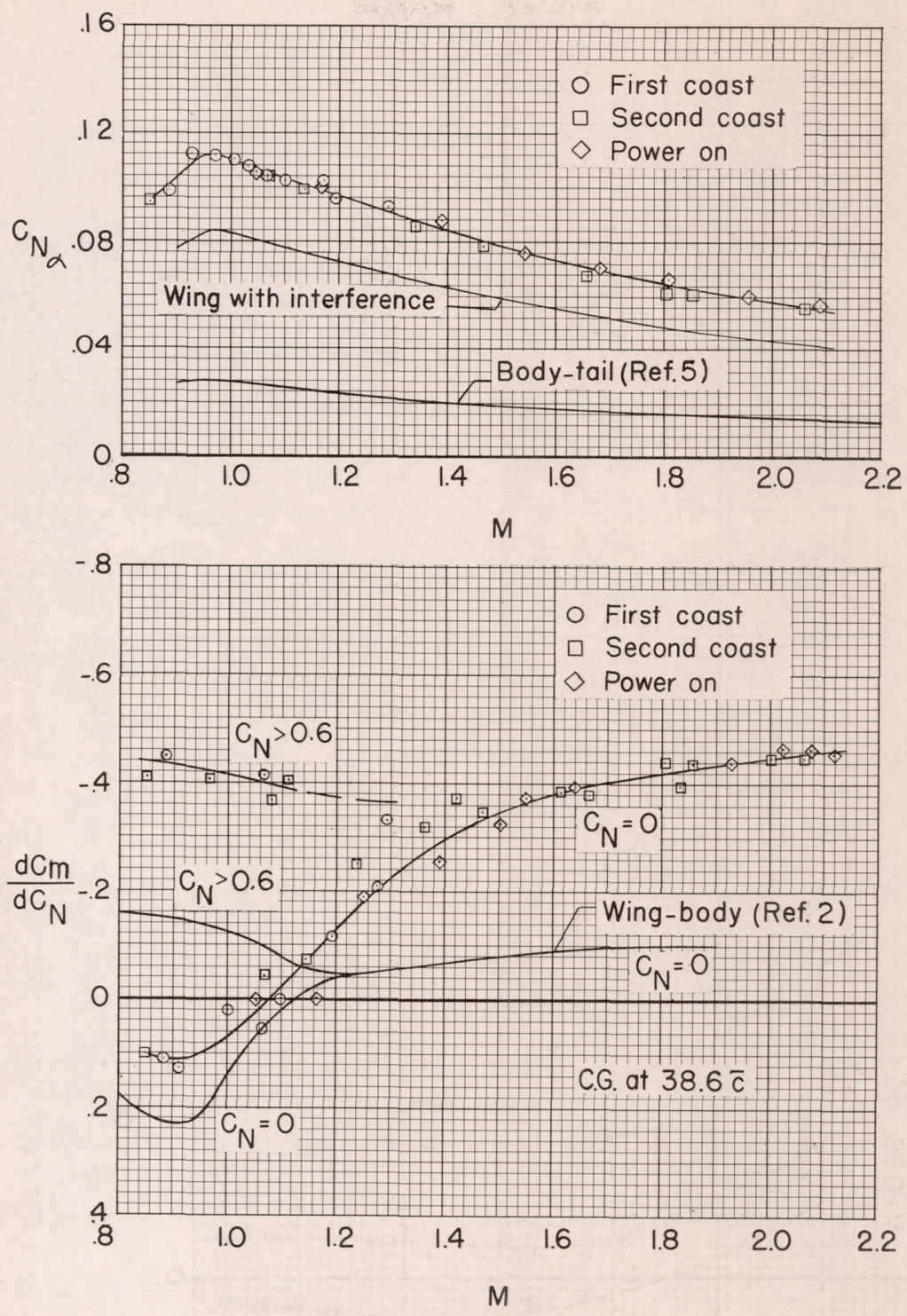


Figure 8.- Power-on and power-off values of $C_{N_\alpha}$ and $\frac{dC_m}{dC_N}$.

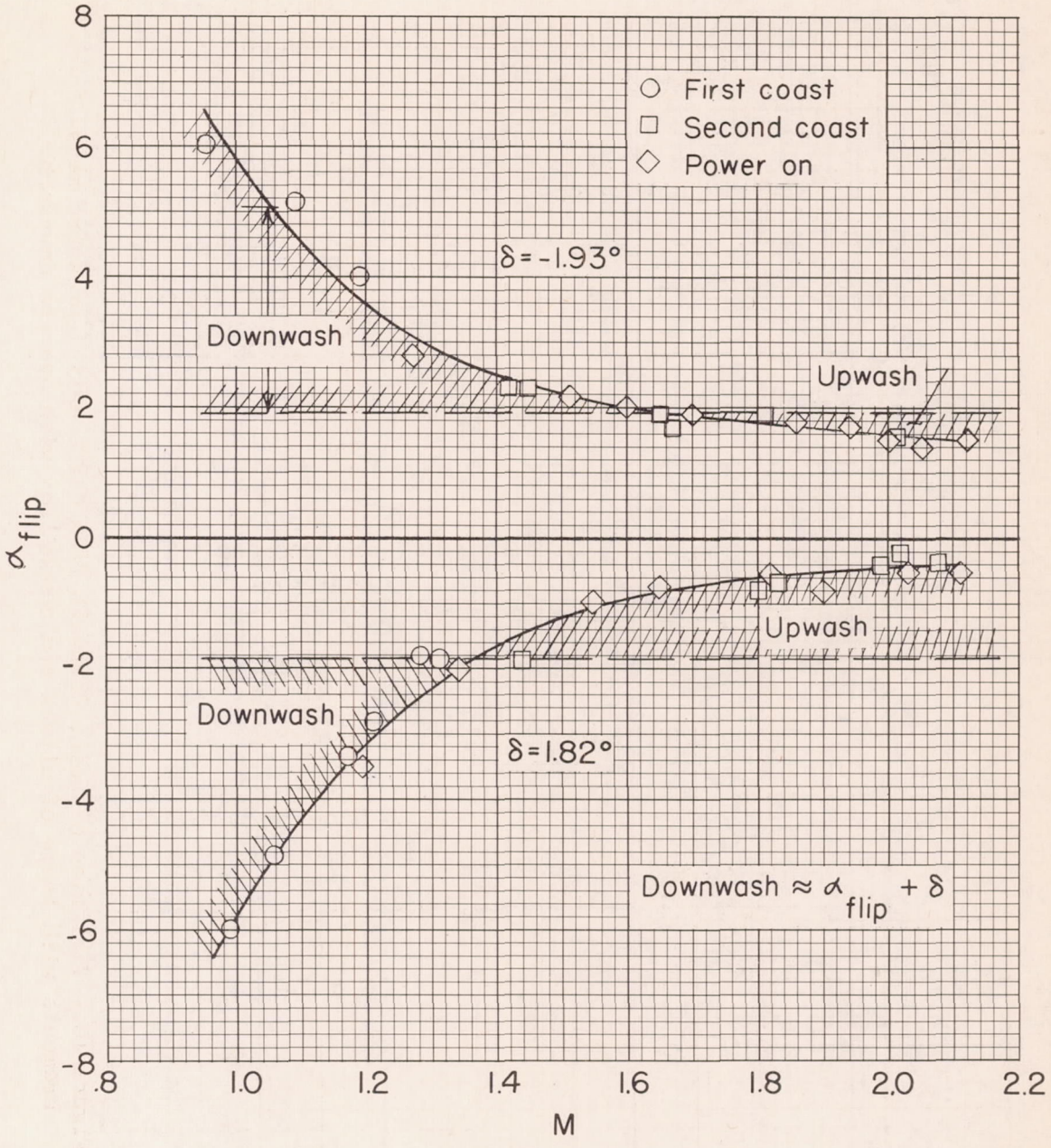


Figure 9.- Downwash and upwash regions indicated by start of tail flip.

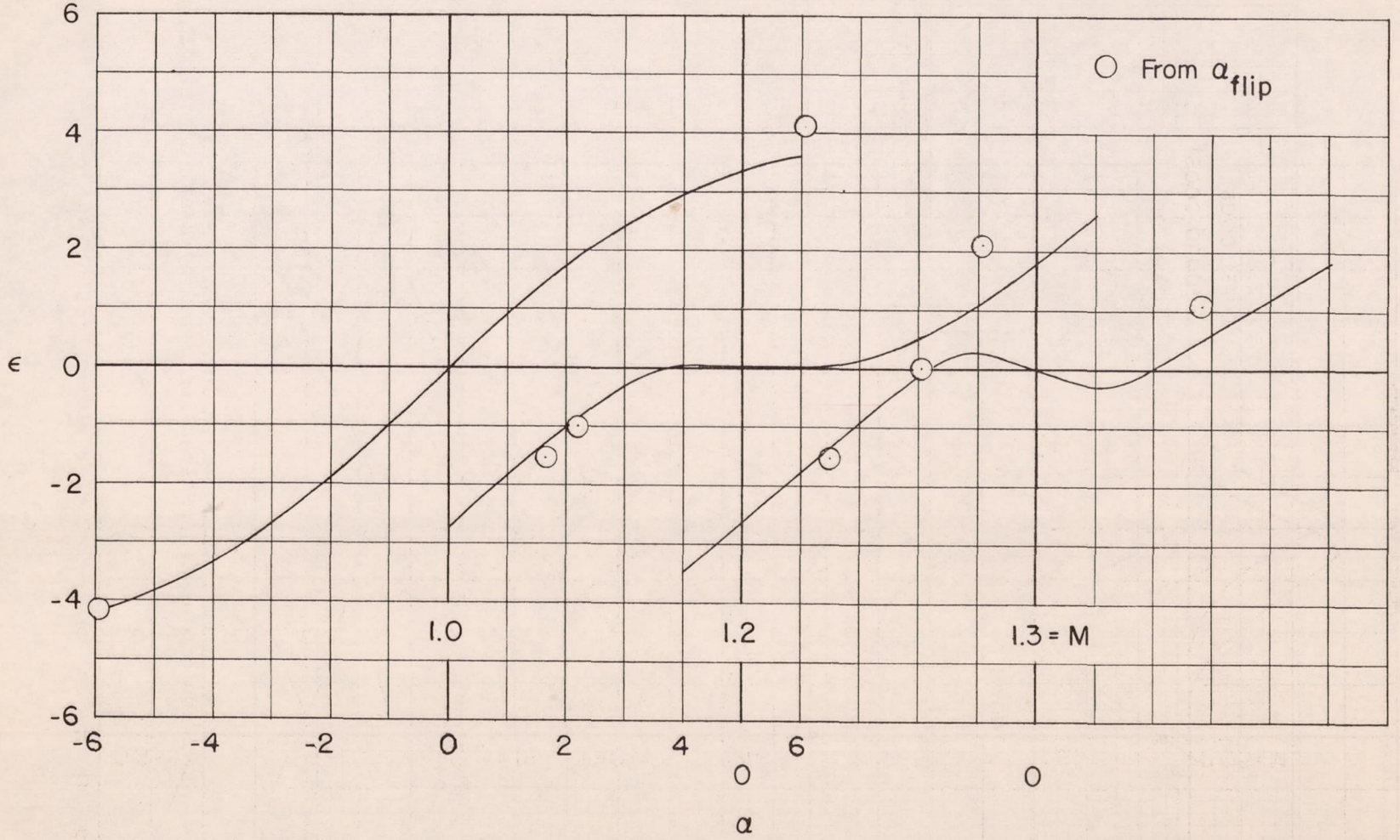


Figure 10.- Variation of point downwash from differential-pressure measurements with angle of attack and comparison with average downwash.

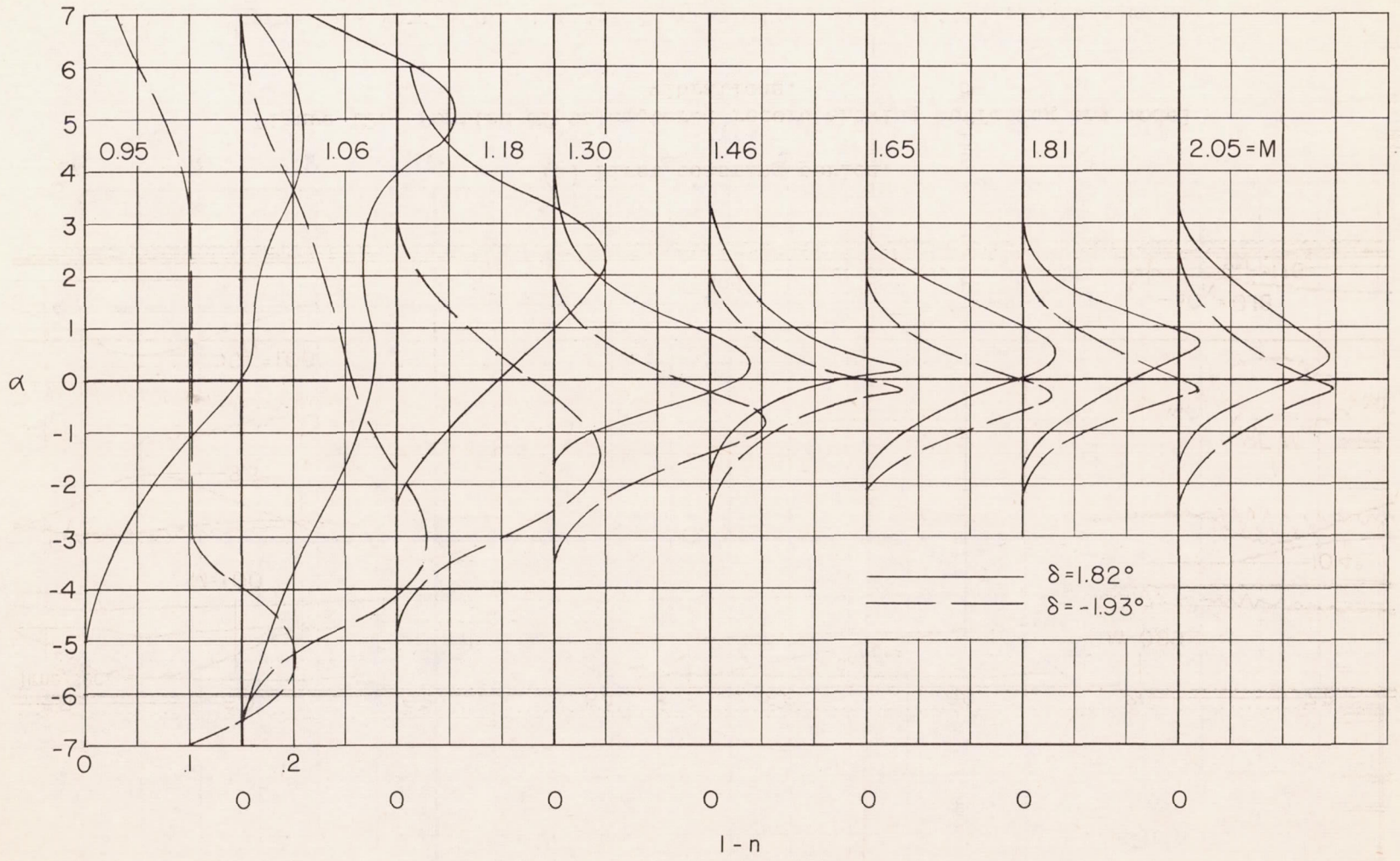


Figure 11.- Pressure loss at the horizontal tail.

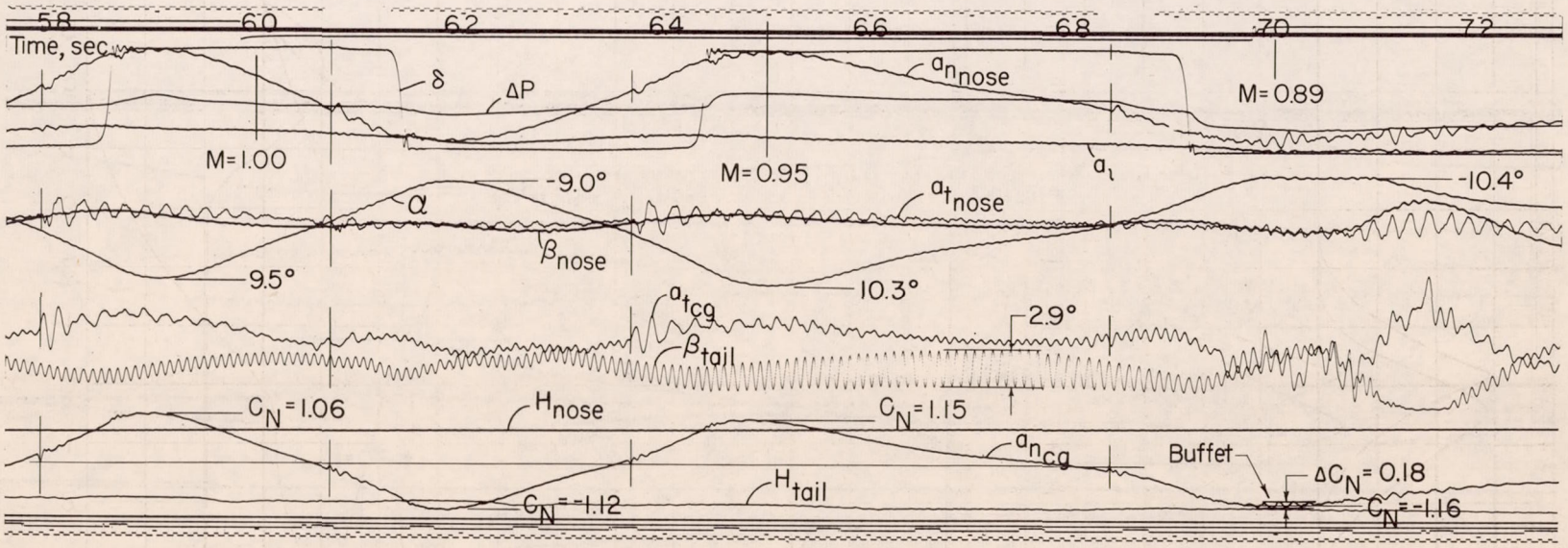


(a) First coasting period.

Figure 12.- Portion of telemetered record showing buffeting and model vibrations.

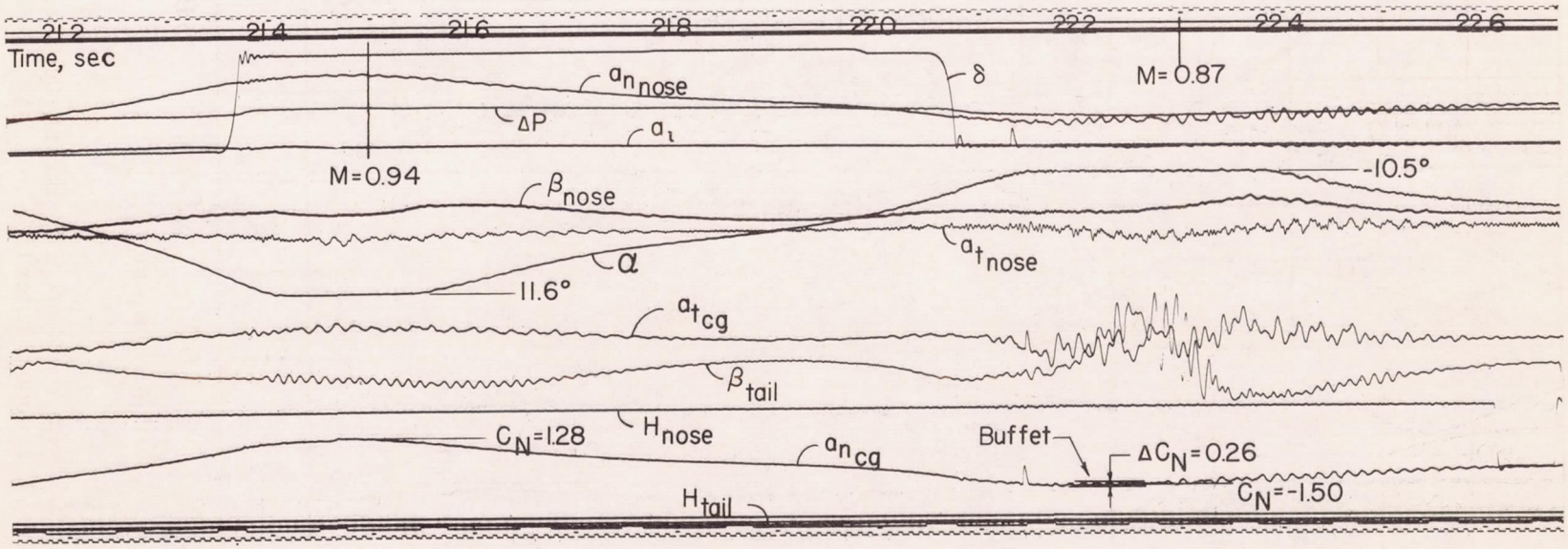


(b) Second coasting period.

Figure 12.- Concluded.

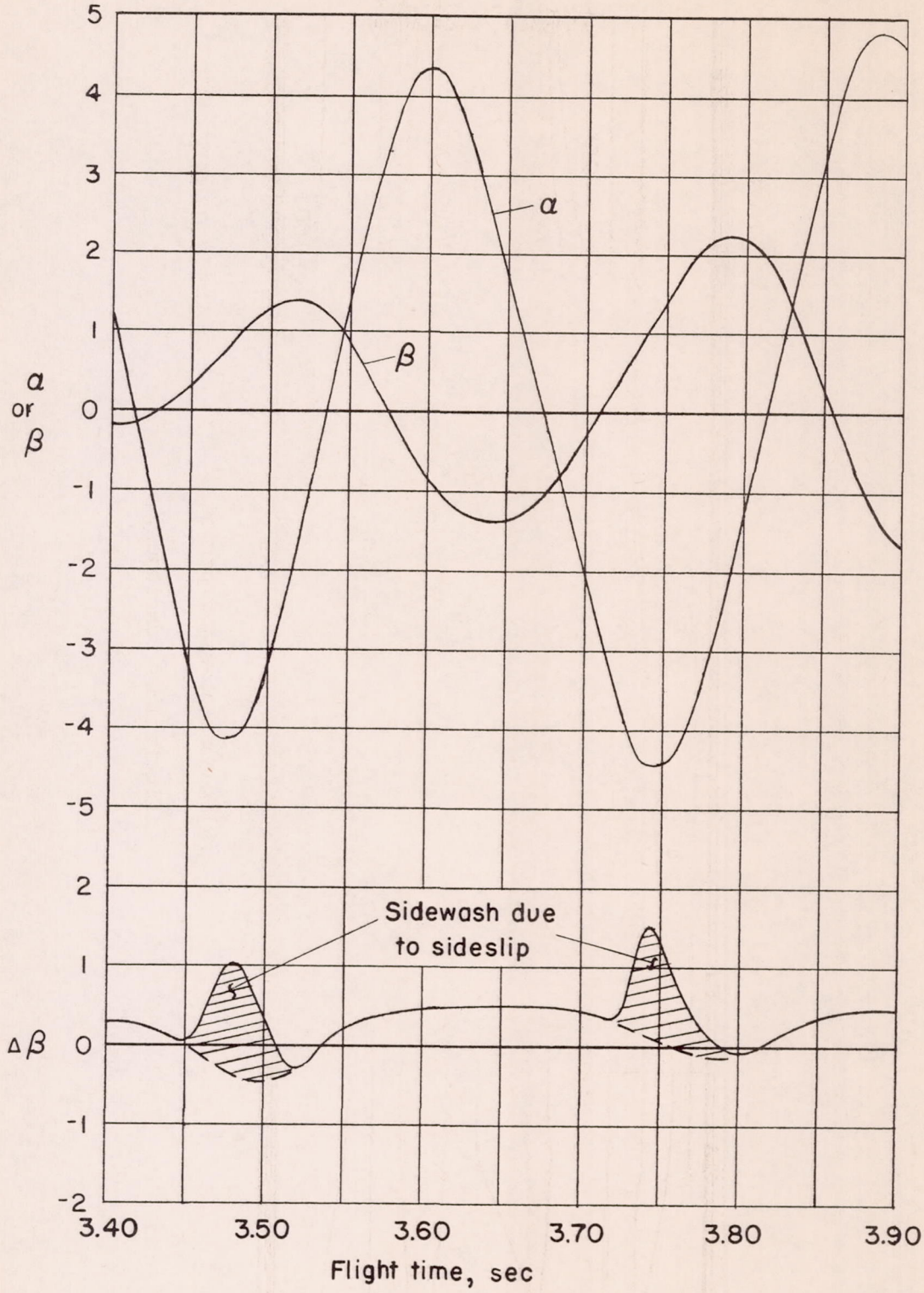


Figure 13.- Sidewash at lower vertical fin during typical buildup of induced sideslip.